Caliphate Journal of Science & Technology (CaJoST)

ISSN: 2705-313X (PRINT); 2705-3121 (ONLINE) Research Article

Open Access Journal available at: https://cajost.com.ng/index.php/files and https://www.ajol.info/index.php/cajost/index

DOI: https://dx.doi.org/10.4314/cajost.v8i1.22

Article Info

Received: 30th January 2026

Revised: 21st March 2026

Accepted: 29th March 2026

[1]Department of Chemistry, National Open University of Nigeria, Abuja, Nigeria
[2]Department of Pure and Industrial Chemistry Sokoto State University, Sokoto, Nigeria
[3]Department of Pharmaceutical and Medicinal Chemistry, Faculty of Pharmaceutical Sciences, Usmanu Danfodiyo University, Sokoto, Nigeria
[4]Nigeria Deposit Insurance Corporation, Sokoto Zonal Office, Sokoto, Nigeria

***Corresponding author's email:**

tomyi2012@yahoo.com

Cite this: *CaJoST*, 2026, 1, 206-217

Corrosion Performance and Adsorption Mechanism of a Green Cu_2O–*Guiera senegalensis* Nanocomposite Coating for Tin in Chloride Media

Thompson Izuagie[1], Umar B. Yabo[2], Ahmad Uba[3], and Shehu Umar[4]

Corrosion of tin-based materials in chloride-rich environments presents a significant challenge for industrial applications, particularly when conventional coatings fail or degrade. In this study, a sustainable nanocomposite anticorrosion coating incorporating Cu_2O nanoparticles and phytochemicals derived from *Guiera senegalensis* was developed and evaluated for corrosion protection of tin substrates in saline media. The nanocomposite coating was formulated by dispersing Cu_2O nanoparticles and aqueous plant extract within an epoxy matrix and applied to tinplate panels. Corrosion resistance was assessed using gravimetric immersion testing in 5 wt% NaCl solution and accelerated salt-spray exposure according to ASTM B117. Phytochemical screening confirmed the presence of glycosides, tannins, flavonoids, saponins, and carbohydrates, which contribute to adsorption-driven inhibition through formation of protective surface films. The nanocomposite coating exhibited significantly lower corrosion rates, reaching a minimum of ~0.17 mm y^{-1} at 1.0 wt% additive loading, compared with ~1.34 mm y^{-1} for the additive-free coating. Salt-spray results showed substantial suppression of rust propagation, with rust-creep lengths below 2 mm and corroded areas below 5% after prolonged exposure. Adsorption isotherm analysis (Langmuir, Temkin, Freundlich, and El-Awady models) indicated spontaneous inhibitor adsorption with $\Delta G°_{ads}$ values between −9 and −12 kJ mol^{-1}, suggesting predominantly physisorption mechanisms. Kinetic modelling further demonstrated that incorporation of Cu_2O nanoparticles significantly reduced corrosion propagation rates and shifted corrosion behaviour toward a barrier-controlled regime. The results highlight the synergistic role of plant-derived inhibitors and nanostructured fillers in producing environmentally friendly, high-performance coatings for corrosion protection of tin in chloride environments.

Keywords: Nanocomposite coating; corrosion inhibition; *Guiera senegalensis*; Cu_2O nanoparticles; adsorption isotherms.

1. Introduction

Corrosion is a pervasive electrochemical process responsible for the gradual degradation of metals when exposed to aggressive environments. It poses significant economic and environmental challenges, with global losses estimated at approximately 3–4 % of the world's gross domestic product (GDP) annually due to infrastructure damage, equipment failure, and maintenance costs.[1] In chloride-rich environments such as marine or saline industrial settings, corrosion of metal substrates is particularly severe because chloride ions accelerate localized attack and destabilize passive films.[2–4] Protective coatings remain one of the most widely adopted strategies for mitigating corrosion because they provide a physical barrier that limits the ingress of oxygen, moisture, and corrosive ions.

Traditional anticorrosion coatings based on chromates, phosphates, and solvent-rich formulations have demonstrated good performance but present environmental and health concerns due to toxicity and volatile organic compound (VOC) emissions.[5] Consequently, increasing attention has been directed toward environmentally benign corrosion-protection technologies, including green corrosion inhibitors and nanocomposite coatings.[1,2,6–9] Nanocomposite systems, in which inorganic nanoparticles are incorporated into organic polymer matrices, can significantly enhance coating durability by improving barrier properties, adhesion, and resistance to permeation of corrosive species.[10–12] Among various nanofillers, silica and metal oxide nanoparticles have attracted considerable interest because they create tortuous diffusion pathways that

slow the transport of aggressive ions and enhance the structural integrity of polymer coatings.[13,14]

In parallel with advances in nanotechnology, plant-derived extracts have emerged as promising green corrosion inhibitors. These natural products typically contain bioactive compounds such as phenolics, flavonoids, tannins, and alkaloids that adsorb onto metal surfaces and form protective molecular films capable of suppressing both anodic metal dissolution and cathodic oxygen reduction reactions.[14–17] The adsorption process is usually driven by π-electron interactions and heteroatom lone pairs, which enable the inhibitor molecules to coordinate with metallic surfaces and reduce electrochemical activity.[18,19] Recent reviews highlight the growing potential of plant extracts as sustainable corrosion inhibitors due to their biodegradability, low toxicity, and wide availability.[8,20]

Recent studies further suggest that combining plant-based inhibitors with nanoscale fillers can produce hybrid coatings that exhibit superior corrosion resistance through synergistic effects. In such systems, the nanoparticles enhance barrier properties and microstructural densification, while the organic constituents adsorb on the metal interface to provide chemical inhibition and passivation.[21–23] These multifunctional nanocomposite coatings can therefore suppress chloride diffusion, reduce coating porosity, and delay underfilm corrosion under aggressive exposure conditions. The integration of green inhibitors with nanostructured fillers also aligns with sustainable materials development and circular-economy principles.

Despite these advances, several critical gaps remain. Although plant-extract-based inhibitors and nanoparticle-reinforced coatings have been widely investigated, particularly for steel and aluminium substrates,[7,8,10–12,24] comparatively limited attention has been given to tin and tinplate materials, which are widely used in packaging and electronics yet exhibit distinct corrosion behaviour in chloride environments. Furthermore, while hybrid systems incorporating plant extracts with nanofillers such as silica and graphene oxide have demonstrated improved performance,[10–13,21,24] there remains limited understanding of how Cu_2O nanoparticles interact synergistically with phytochemical constituents to influence adsorption thermodynamics and corrosion kinetics.[22,23,25] In addition, although numerous plant extracts have been explored as green corrosion inhibitors,[7,8,14,17] the use of *G. senegalensis*, a phytochemically rich and locally abundant plant in Sub-Saharan Africa, has not been systematically investigated in nanocomposite coating systems for corrosion protection, despite its demonstrated bioactive potential.[26]

In this study, we address these gaps by developing a Cu_2O–*G. senegalensis* nanocomposite coating and evaluating its corrosion protection performance on tin substrates in chloride media. The work provides new insights into (i) the synergistic coupling of nanoparticle-induced barrier effects and phytochemical adsorption, (ii) the transition of corrosion kinetics from diffusion-controlled to barrier-controlled regimes, and (iii) the adsorption thermodynamics governing inhibitor–surface interactions. These contributions advance the design of sustainable, plant-based nanocomposite coatings tailored for chloride-induced corrosion environments.

2. Materials and Methods

2.1 Materials and Instrumentations

Analytical-grade reagents were used throughout the study. *G. senegalensis* leaves were obtained from Dukamaje area of Yabo Local Government, Sokoto State, Nigeria. The Cu_2O-nanoparticles used in this study were samples previously prepared using aqueous neem leave extract and characterized using Fourier Transform Infrared Spectroscopy (FTIR), X-ray Diffraction (XRD), and Scanning Electron Microscopy (SEM) as previously reported elsewhere.[27] The epoxy resin system (two-pack resin + hardener; PPG Industries) served as the polymeric matrix. Chemicals used included sodium hydroxide (NaOH, 99.0 %), sodium chloride (NaCl, 99.5 %), hydrochloric acid (HCl, 36 %), n-hexane (99.0%), all supplied by Qualikems India, JHD China and Sigma Aldrich. Distilled water was used for washing and solution preparation. Equipment used in this study included a muffle furnace (Narange Medical Ltd., India), vacuum oven (Gallenkamp, UK), analytical balance (OHAUS SPU-202, USA), a fabricated salt-spray accelerated corrosion test chamber (see Figure 1), paint plastic mixing cups (LAKGRUPPEN, Denmark), tinplate test panels (Pro Test Panels Ltd., England), and a Dino-Lite digital microscope (AM2011, Scitek Global Co., Ltd., China).

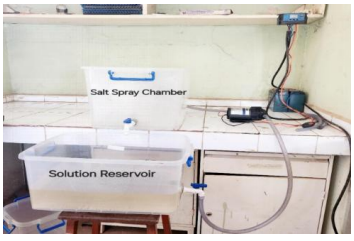

Figure 1: Fabricated laboratory salt-spray accelerated corrosion testing setup showing the salt spray chamber (upper container) and solution reservoir (lower container) connected through a pumping system used to generate a continuous saline mist for coating durability evaluation under simulated marine conditions.

2.2 Pretreatment, extraction and screening of *G. senegalensis leaves*

Fresh leaves of *G. senegalensis* were collected, washed with distilled water to remove surface contaminants, and shade-dried at ambient

temperature. The dried leaves were then pulverized into a fine powder using a laboratory grinder. Approximately 100 g of the powdered plant material was transferred into a clean conical flask and extracted with 1000 mL of distilled water by boiling for 1 h. The mixture was allowed to cool to room temperature and subsequently filtered first through cotton wool and then through Whatman filter paper to remove particulate matter. The resulting filtrate was concentrated and dried using freeze-drying to obtain the crude aqueous extract.[26] The dried extract was stored in airtight containers at 4 °C until further use. Phytochemical screening followed standard colour-test procedures: Dragendorff's reagent for alkaloids; ferric-chloride for phenolics/tannins; Shinoda reagent for flavonoids; and Kedde's reagent for glycosides.[18,19]

2.3 Formulation of Cu_2O-Nanocomposite Coating

The nanocomposite was formulated by blending Cu_2O-nanoparticles and *G. senegalensis* extract with the epoxy resin at a mass ratio of 4:1 (nanoparticles: extract). The resin: hardener ratio was 80: 20. The mixture was mechanically stirred for 10 min to achieve homogeneous dispersion. The dispersion quality was visually assessed during mixing and after curing based on coating uniformity and absence of macroscopic agglomerates. Coatings were applied to degreased tin-plate panels (50 × 25 × 1 mm) using a film applicator and cured at ambient temperature for 24 h. Similar epoxy/nanoparticle and plant-extract hybridizations have been reported.[28]

2.4 Corrosion Resistance Evaluation

Corrosion performance was assessed using gravimetric immersion tests in 5 wt% NaCl and accelerated salt-spray testing (ASTM B117-23), combined with surface examination to evaluate corrosion resistance and coating durability under simulated marine conditions.

2.4.1 Immersion Test

Immersion experiments were conducted using coatings containing varying additive concentrations (0.5–1.5 wt%). The prepared samples were immersed in a 5 wt% NaCl solution at room temperature for 90 days. At predetermined intervals, the specimens were removed, cleaned, dried, and weighed to determine mass loss. Corrosion rate (CR) was calculated by:

$$CR = \frac{87.6 \times W}{D \times A \times T}$$

where W = weight loss (mg), D = density (g cm^{-3}), A = area (cm^2), T = time (h).[25]The inhibition efficiency (η %) was derived as:

$$\eta = \frac{CR_0 - CR_i}{CR_0} \times 100$$

where CR_0 = corrosion rate without inhibitor and CR_i = rate with inhibitor.[10]

2.4.2 Accelerated Salt-Spray Test and Surface Examination

Corrosion performance of the coated and X-scribed panels was evaluated according to ASTM B117-23.[29] Samples were exposed to a continuous 5 wt % NaCl fog at 35 °C and 95 % relative humidity in a salt-spray chamber. At scheduled intervals (24, 48, 72, 96, 168, 240 and 360 h), panels were withdrawn, rinsed with deionized water, and air-dried for image analysis. Surface degradation was documented using a digital optical microscope (10×–200×, reflected bright-field illumination) following ASTM D1654 procedures.[30] Micrographs of the scribed regions were captured at fixed magnification and lighting to record rust propagation, blistering, and coating breakdown. Image analysis provided rust-creep length and corroded-area fraction, while time-to-first-rust and extent of film deterioration were noted visually. Prolonged resistance to rust initiation and lower rust-creep or corroded-area values were taken as indicators of superior coating protection.[30]

2.5 Adsorption Behaviour and Corrosion Kinetics

Adsorption behaviour of the additives on the metal surface was evaluated using Langmuir, Temkin, Freundlich, and El-Awady adsorption isotherm models. Surface coverage (θ) values were calculated from corrosion rate data and fitted to the linearized forms of the respective isotherms to assess the adsorption characteristics and interactions between inhibitor molecules and the metal surface. The equilibrium adsorption constant (K_{ads}) obtained from the isotherm plots was used to estimate the standard free energy of adsorption ($\Delta G°_{ads}$) using $\Delta G^{\circ}_{ads} = -RT\ln(55.5K_{ads})$, where R is the gas constant and T is the absolute temperature. The magnitude of $\Delta G°_{ads}$ was used to infer the adsorption mechanism.[31] Time-dependent rust-creep data were further analysed to investigate corrosion kinetics. The data were fitted to the parabolic diffusion model $(L^2 = k_p t + C)$and the power-law model $(L = kt^n)$. Regression parameters (k_p, k, n) and goodness-of-fit (R^2) were used to determine whether corrosion progression was diffusion-controlled, interface-controlled, or governed by mixed kinetics. [32]

2.6 Data Analysis

All tests were performed in triplicate. Data were expressed as mean ± standard deviation, and comparisons among coatings were made using one-way ANOVA ($p < 0.05$). Figures and statistical plots were generated using OriginPro 2024.

3. Results and Discussion

3.1 Phytochemical screening of *G. senegalensis*

Phytochemical screening of aqueous extract of leaves of *G. senegalensis* revealed glycosides, tannins, flavonoids, saponins, and carbohydrates (Table 1). These bioactive compounds possess π-systems and heteroatom functional groups that enable physisorption or chemisorption on metal surfaces, forming compact protective films that suppress anodic dissolution and cathodic oxygen reduction.[1] Their antioxidant properties also limit ROS pathways.[18,19] Collectively, these constituents can synergistically interact with CuO nanoparticles to enhance coating compactness, reduce porosity, and improve corrosion protection of tin in chloride environments.[33]

Table 1. Phytochemical screening of aqueous extract of leaves of *G. senegalensis*

Constituents	Saponins	Tannin	Glycosides	Steroids	Flavonoids	Anthraquinones	Terpenoids	Carbonhydrates
Inference	+	+	+	-	+	-	-	+

Key: (+) = Detected, (-) = Not Detected

3.2 Preparation of Cu_2O nanocomposite coating

The Cu_2O-nanocomposite coating was prepared using Cu_2O previously prepared and characterised as described elsewhere.[27] The initially amber epoxy mixture darkened to a brownish colour upon the addition of the nanoparticles. Visible agglomerates were initially observed; however, thorough stirring reduced these clusters and produced a more uniform dispersion. The blend also became noticeably more viscous than the neat epoxy, indicating interactions between the nanoparticles and the polymer matrix. The system exhibited slight resistance to flow and required additional mixing effort to achieve homogeneity. A sample of the resulting coating on a tin plate is shown in Figure 2.

Figure 2. A coated tinplate test panel showing the prepared coating formulation after application and curing prior to corrosion testing.

3.3 Corrosion-Resistance Performance

3.3.1 Immersion Testing

The immersion experiments were performed with varying additive concentrations (0.5–1.5 wt%), and the prepared samples were immersed in a 5 wt% NaCl solution at room temperature for a period of 90 days.

(a). Effect of additive concentrations

Figure 3 shows the variation of corrosion rate with additive concentration for plant-extract-modified and nanocomposite-modified coatings compared with the additive-free coating. The unmodified sample exhibits a high corrosion rate (~1.34 mm y^{-1}), indicating poor resistance in chloride environments. Incorporation of the plant extract significantly reduces corrosion rates from ~0.67 mm y^{-1} at 0.5 wt% to ~0.56 mm y^{-1} at 1.5 wt%, reflecting improved surface coverage and adsorption-driven protective film formation by phytochemicals.[8,33]

Cu_2O-based nanocomposite coatings show markedly lower corrosion rates, reaching a minimum of ~0.17 mm y^{-1} at 1.0 wt%, representing the optimum loading. This enhanced protection is attributed to nanoparticle barrier effects that block pores and limit chloride diffusion. [21,22] A slight increase at 1.5 wt% (~0.22 mm y^{-1}) likely results from nanoparticle agglomeration. Overall, nanocomposite coatings outperform plant-extract systems, consistent with reports on green nanocomposite anticorrosive coatings.[23]

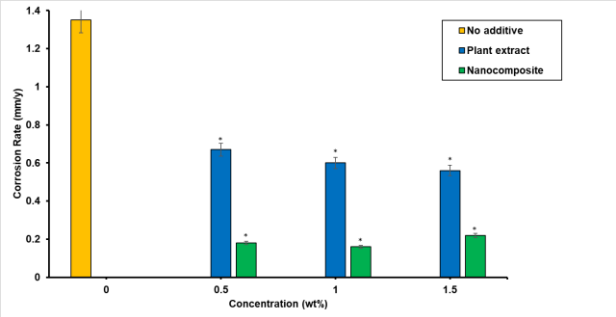

Figure 3: Corrosion rate of tin substrates coated with plant extract and Cu_2O nanocomposite formulations at varying concentrations in 5 wt% NaCl solution. Error bars represent standard deviation (n = 3). Statistical significance relative to the unmodified coating is indicated as * ($p < 0.05$).

(b). Time-resolved corrosion performance

The time-resolved corrosion rates and inhibition efficiencies for the uncoated and coated specimens are presented in Figures 4 and 5 respectively. Uncoated metal showed consistently high corrosion rates (~0.00135–0.00140 g/day) during 90-day immersion in 5 wt% NaCl, indicating minimal protection. In contrast, coatings containing plant extract and nanocomposite additives significantly reduced corrosion. The plant-extract coating decreased the rate to ~0.00075 g/day, while the

nanocomposite coating showed the lowest and most stable rate (~0.00065 g/day). After 90 days, inhibition efficiencies were ~54–58% for the plant extract and ~87–90% for the nanocomposite coating. The improved performance is attributed to protective adsorption films from plant phytochemicals and enhanced barrier effects from nanoscale fillers that restrict ion transport and corrosion reactions. These findings align with studies reporting the effectiveness of green corrosion inhibitors and nanocomposite coatings in saline environments.[8,20,23] Thus, the nanocomposite coating provides superior corrosion protection, while plant extracts offer environmentally friendly inhibition with moderate efficiency.

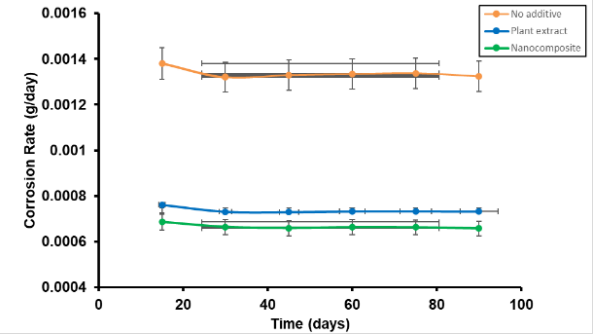

Figure 4: Time-dependent corrosion rates of tin substrates coated with plant extract and Cu_2O nanocomposite formulations in 5 wt% NaCl solution. Error bars represent standard deviation (n = 3).

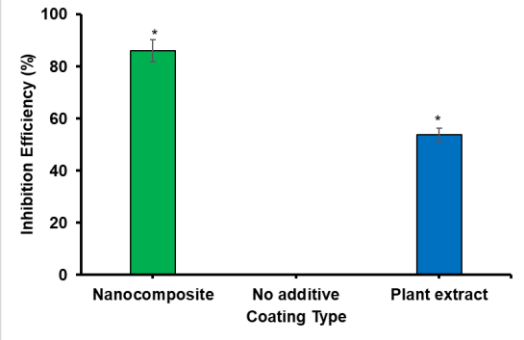

Figure 5: Inhibition efficiency of tin substrates coated with plant extract and Cu_2O nanocomposite formulations. Error bars represent standard deviation (n = 3). Statistical significance relative to the unmodified coating is indicated as * ($p < 0.05$).

3.3.2 Salt-spray (fog) exposure

The corrosion performance of the coated tin panels was also evaluated using an accelerated salt-spray (fog) test in 5 wt% NaCl in accordance with ASTM B117. The degradation behaviour was assessed qualitatively by optical micrographs of X-scribed regions (Figure 6) and quantitatively using corroded area fraction (Figure 7) and rust-creep length from the scribe (Figure 8). These results are summarized in Table 2.

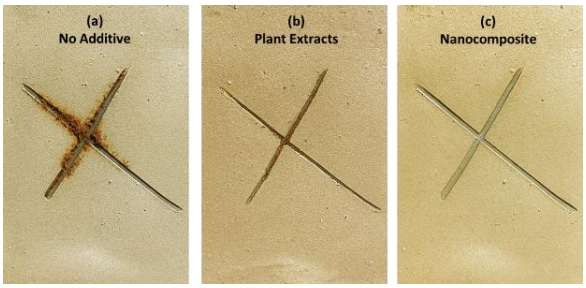

Figure 6: Optical micrographs of X-scribed coated tin panels after exposure to a 5 wt% NaCl salt-spray environment (ASTM B117), showing scribe-region corrosion for (a) no additive, (b) plant-extract additive, and (c) Cu_2O-based nanocomposite coating.

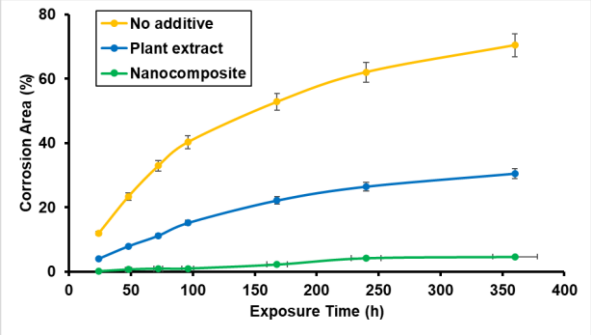

Figure 7: Evolution of corroded area (%) of X-scribed tin panels coated with no additive, plant extract, and Cu_2O-based nanocomposite coatings as a function of exposure time in 5 wt% NaCl salt-spray environments. Error bars represent standard deviation (n = 3).

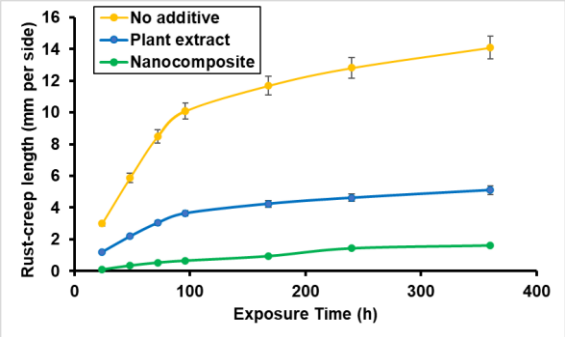

Figure 8: Rust-creep length (mm per side) of X-scribed tin panels coated with no additive, plant extract, and Cu_2O-based nanocomposite coatings as a function of exposure time in a 5 wt% NaCl salt-spray environment. Error bars represent standard deviation (n = 3).

Table 2: Summary of rust-creep length, corroded-area fraction, and corrosion-severity interpretation for tin panels coated with no additive, plant extract, and Cu_2O-based nanocomposite formulations after salt-spray exposure.

Coating Type	Rust-Creep Length (mm)	Corroded-Area Fraction (%)	Interpretation
No Additive	12.0 ± 2.0	65.0 ± 5.0	Very severe corrosion
Plant Extract	4.0 ±	25.0 ± 5.0	Moderate

	1.0			improvement
Nanocomposite	1.2 0.5	±	3.0 ± 2.0	Excellent inhibition

Values = mean ± standard deviation.

Figure 6 presents the optical micrographs of the scribed coatings after salt-spray exposure. The no-additive coating (Figure 6a) shows extensive rust formation along the scribe and pronounced underfilm corrosion, indicating rapid electrolyte ingress and poor barrier integrity once the coating is breached. In contrast, the plant-extract-modified coating (Figure 6b) exhibits visibly reduced corrosion staining and shorter rust creep, suggesting partial inhibition of anodic and cathodic reactions through adsorption-driven surface protection. The Cu_2O-based nanocomposite coating (Figure 6c) demonstrates the best performance, with minimal corrosion products and stable scribe edges, reflecting superior resistance to underfilm corrosion and enhanced coating compactness. These qualitative observations align with established corrosion-protection mechanisms whereby nanofillers decrease coating porosity and increase diffusion tortuosity for aggressive ions, while phytochemicals form interfacial protective films through donor–acceptor interactions.[5,8,22,34]

The quantitative progression of corroded area (%) with exposure time is shown in Figure 7. The no-additive coating exhibits a steep increase in corroded area from approximately 12% at early exposure to nearly 70% after prolonged exposure, confirming rapid coating failure under chloride attack. The plant-extract coating shows a substantially slower corrosion progression, with corroded area increasing from about 4% to approximately 30% over the same period. In contrast, the nanocomposite coating maintains a remarkably low corroded area, rising only marginally from near-zero to approximately 5% even after extended exposure. This pronounced improvement demonstrates the synergistic barrier effect of Cu_2O nanoparticles within the polymer matrix, which block micro-pores, restrict chloride diffusion, and reinforce coating cohesion. Similar trends have been widely reported for nanoparticle-reinforced coatings, where reduced permeability and enhanced microstructural stability significantly delay underfilm corrosion.[24]

Figure 8 depicts the time-dependent evolution of rust-creep length from the scribe for all coating systems. The no-additive coating shows rapid and continuous rust propagation, reaching approximately 14 mm per side after prolonged exposure. The plant-extract coating exhibits moderated rust creep, increasing gradually from about 1.2 mm to around 5 mm, confirming that phytochemicals provide measurable inhibition but do not fully suppress underfilm corrosion. Notably, the nanocomposite coating displays the smallest rust-creep length throughout the test, remaining below approximately 2 mm even at the longest exposure time. This superior scribe-edge stability reflects strong interfacial adhesion, reduced electrolyte transport pathways, and enhanced resistance to cathodic delamination—mechanisms commonly attributed to nanofiller-modified coatings.[5,22,24,34]

Collectively, the salt-spray results establish a clear protective hierarchy: Nanocomposite coating > Plant-extract coating > No-additive coating. The plant-extract additive improves corrosion resistance through adsorption-driven film formation and surface passivation, consistent with the known behaviour of polyphenol- and alkaloid-rich inhibitors.[8] However, the Cu_2O nanocomposite coating provides substantially superior protection by combining chemical inhibition with physical barrier reinforcement and microstructural densification. These findings are in strong agreement with recent studies on green nanocomposite coatings, which report marked reductions in rust creep, corroded area, and coating failure rates relative to organic inhibitors alone.[23]

Importantly, the delayed rust initiation, reduced corroded area, and minimal rust-creep length observed for the nanocomposite system demonstrate its suitability as a high-performance, eco-friendly corrosion-protection strategy for tin substrates in chloride-rich environments.

Although detailed characterization of the Cu_2O nanoparticles was reported previously, their distribution within the epoxy matrix in the present study appears relatively uniform based on the observed coating homogeneity and enhanced corrosion performance. The significant reduction in corrosion rate and improved salt-spray resistance suggest effective nanoparticle dispersion with minimal large-scale agglomeration. Furthermore, the increased viscosity during mixing and absence of visible phase separation support strong interfacial interactions, consistent with well-dispersed nanofillers that promote matrix densification, increased diffusion tortuosity, and improved barrier properties.

3.4 Mechanism of Corrosion protection

3.4.1. Adsorption Isotherm and Thermodynamic Analysis

To elucidate the adsorption behaviour of the corrosion inhibitors on the tin surface, the experimental inhibition data were fitted to multiple adsorption isotherm models, including Langmuir, Temkin, Freundlich, and El-Awady (Figure 9). The corresponding isotherm parameters are summarized in Table 3, while derived adsorption constants and thermodynamic parameters using the Langmuir isotherm are presented in Table 4.

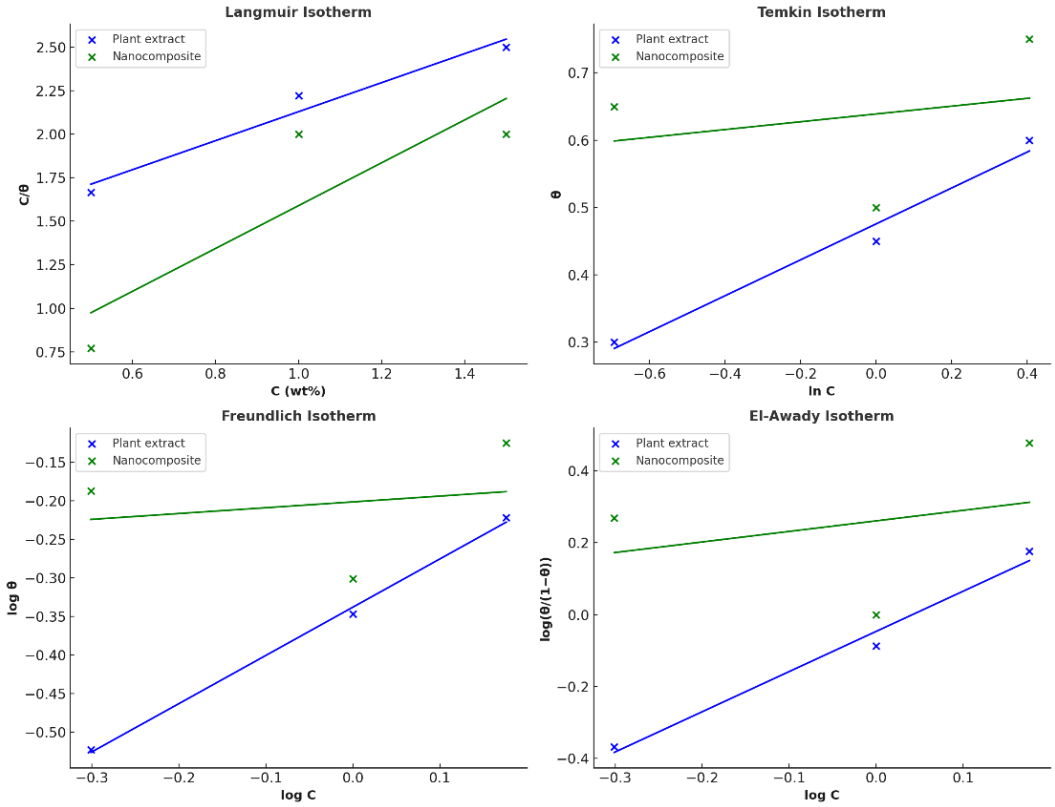

Figure 9: Comparative adsorption isotherms (Langmuir, Temkin, Freundlich, and El-Awady) illustrating the surface-adsorption behaviour of plant extract and Cu_2O nanocomposite inhibitors on tin in a chloride medium.

Table 3: Isotherm fitting parameters (slope, intercept, and correlation coefficient, R^2) for Langmuir, Temkin, Freundlich, and El-Awady adsorption models of plant extract and Cu_2O-based nanocomposite inhibitors on tin in 5 wt% NaCl solution.

Isotherm Model	Inhibitor	Slope	Intercept	R^2
Langmuir	Plant extract	0.708	1.350	0.991
Langmuir	Nanocomposite	0.939	0.520	0.980
Temkin	Plant extract	0.299	0.456	0.998
Temkin	Nanocomposite	0.138	0.647	0.981
Freundlich	Plant extract	0.373	−0.463	0.992
Freundlich	Nanocomposite	0.191	−0.214	0.963
El-Awady	Plant extract	0.697	−0.372	0.993
El-Awady	Nanocomposite	0.195	0.229	0.958

Table 4: Thermodynamic adsorption parameters derived from the Langmuir isotherm for plant extract and Cu_2O nanocomposite inhibitors on tin, indicating adsorption strength, spontaneity, and stability of the adsorbed layer.

Inhibitor	Intercept (b)	K_{ads} (L/mol)	$\Delta G°_{ads}$ (kJ/mol)	Interpretation
Plant extract	1.350	0.741	–9.21	Weak physisorption; spontaneous
Nanocomposite	0.520	1.923	–11.56	Stronger physisorption; more stable adsorbed layer

(a). Isotherm Model Fitting

The goodness of fit (R^2) shown in Table 5 indicates that multiple isotherms reasonably describe the adsorption process for both inhibitors. In particular, high R^2 values for the Langmuir and Temkin models for the plant extract (R^2 ~0.99) suggest that adsorption occurs predominantly as a monolayer with a uniform distribution of active sites and moderate adsorbate–surface interactions. Langmuir behaviour implies that each inhibitor molecule occupies a distinct active site, supporting a single-site binding mechanism common in corrosion inhibition studies. The concept of Langmuir monolayer adsorption is well established in surface

science and has been widely applied to inhibitor adsorption analyses in corrosive media.[14]

The fit to the Freundlich model further indicates heterogeneous adsorption characteristics, where surface energy sites vary in affinity, especially for larger, multi-component organic extracts. The El-Awady and Temkin fits, with slightly lower but still significant R^2 values, imply that lateral interactions and adsorbate–adsorbate effects also contribute to the overall adsorption behaviour, consistent with previous corrosion inhibitor studies.[35]

(b). Adsorption Equilibrium and ΔG° ads Interpretation

The adsorption equilibrium constants (K_{ads}) and corresponding standard free energy of adsorption ($\Delta G°_{ads}$) values (Table 6) provide insight into the strength and spontaneity of inhibitor adsorption. Both the plant extract and nanocomposite inhibitors exhibit negative $\Delta G°_{ads}$ values, confirming that adsorption onto the tin surface is spontaneous under the test conditions. Negative free energies reflect a thermodynamically favourable inhibitor adsorption process, in line with other corrosion inhibition studies where $\Delta G°_{ads}$ values indicate spontaneous surface coverage.[36]

The magnitude of ΔG°ads provides qualitative insight into the adsorption mechanism. While conventional thresholds (≈−20 kJ mol^{-1} for physisorption and <−40 kJ mol^{-1} for chemisorption) should be interpreted cautiously, the values obtained here (−9 to −12 kJ mol^{-1}) indicate predominantly physisorbed inhibition layers. This suggests that adsorption is governed mainly by electrostatic interactions, van der Waals forces, and hydrogen bonding between phytochemical functional groups (e.g., –OH, C=O, π-systems) and the tin surface. However, within the coating system, these interactions are complemented by microstructural effects, where phytochemicals accumulate at the metal/coating interface and contribute to film formation. The absence of more negative ΔG°ads values (<−40 kJ mol^{-1}) indicates that strong chemisorption is not dominant, and corrosion protection arises primarily from interfacial adsorption coupled with barrier effects. These effects are inferred from performance trends and literature, and require further electrochemical or surface characterization for direct confirmation.

Importantly, the nanocomposite inhibitor exhibits a higher K_{ads} and more negative $\Delta G°_{ads}$ than the plant extract alone, indicating a more stable and stronger physisorbed layer. This aligns with its superior performance in corrosion protection tests, where enhanced surface coverage and barrier action are expected due to synergistic interactions between the nanophase particles and organic constituents.

(c). Mechanistic Insights

The combination of isotherm model fitting and thermodynamic parameters suggests a multi-faceted adsorption mechanism for the inhibitors studied:

i. The Langmuir-type behaviour and high R^2 values indicate that the initial adsorption stage involves monolayer formation with limited lateral interactions.

ii. Freundlich and Temkin fits point to surface heterogeneity and adsorbate-adsorbate effects, which are plausible given the complex composition of plant extracts and nanocomposite surfaces.

iii. Negative $\Delta G°_{ads}$ confirms spontaneous adsorption, with more favourable energies for the nanocomposite indicating enhanced surface affinity and stability of the adsorbed film.

These results corroborate recent corrosion inhibition studies that use adsorption isotherms to clarify how inhibitors bind to metal surfaces and how that binding correlates with protective efficiency.[35]

3.4.2. Kinetic Analysis

To further investigate the corrosion kinetics, the corrosion-protection mechanisms of the coated tin substrates were analyzed using kinetic models derived from accelerated salt-spray exposure in 5 wt% NaCl. The evolution of rust growth was examined through parabolic rate plots (L^2 vs. time; Figure 10) and power-law plots (ln L vs. ln t; Figure 11), while the corresponding kinetic parameters were extracted from model fitting (Table 6).

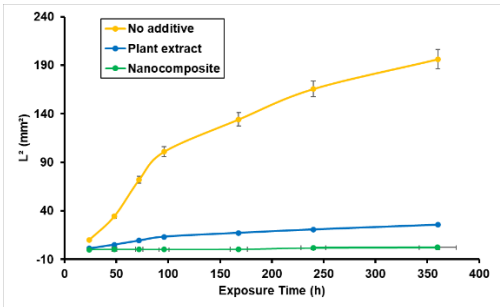

Figure 10: Parabolic rate plots showing corroded area parameter, L^2 (mm^2) versus exposure time (h) for unmodified, plant-extract-modified, and Cu_2O nanocomposite-modified coatings on tin in 5 wt% NaCl salt spray. Error bars represent standard deviation (n = 3).

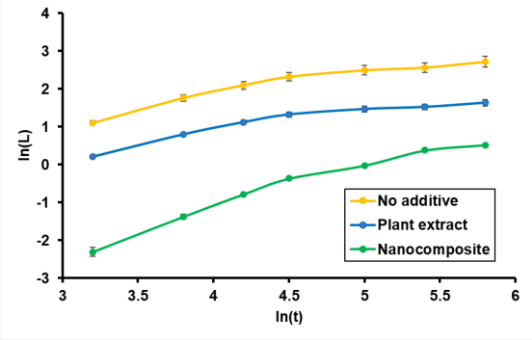

Figure 11: Power law plots showing ln(L) as a function of ln(t) for unmodified, plant-extract-modified, and Cu_2O nanocomposite-modified coatings on tin in a 5 wt% NaCl salt-spray environment. Error bars represent standard deviation (n = 3).

Table 5: Kinetic fit parameters (parabolic and power-law) for rust growth of epoxy coatings with no additives, plant extract and nanocomposite.

Sample	Model	Rate Constant	Exponent (n)	R^2
No Additives	Parabolic	k_p = 0.8521 mm $h^{-½}$	–	0.884
Plant Extract	Parabolic	k_p = 0.3106 mm $h^{-½}$	–	0.878
Nanocomposite	Parabolic	k_p = 0.0626 mm $h^{-½}$	–	0.731
No Additives	Power Law	$k = e^{-0.37} \approx 0.693$	0.542	0.842
Plant Extract	Power Law	$k = e^{-1.23} \approx 0.291$	0.512	0.868
Nanocomposite	Power Law	$k = e^{-5.43} \approx 0.004$	1.052	0.896

Figure 10 shows that the corroded-area parameter (L^2) increases approximately linearly with exposure time for all coating systems, indicating that rust propagation follows parabolic kinetics—a hallmark of diffusion-controlled corrosion processes. The parabolic rate constants (k_p) derived from the fits (Table 6) reveal a pronounced reduction in corrosion growth rate upon additive incorporation. The no-additive coating exhibits the highest k_p (0.8521 mm $h^{-½}$), reflecting rapid chloride diffusion and weak barrier integrity. In contrast, the plant-extract coating shows a substantially lower k_p (0.3106 mm $h^{-½}$), confirming that phytochemical constituents retard ionic transport and partially suppress rust growth.

Most notably, the Cu_2O-based nanocomposite coating displays the smallest parabolic rate constant (k_p = 0.0626 mm $h^{-½}$), corresponding to nearly an order-of-magnitude reduction relative to the no-additive system. This dramatic decrease highlights the strong barrier effect imparted by nanoscale fillers, which increase diffusion tortuosity, block micro-pores, and densify the polymeric matrix. Similar parabolic trends and rate-constant suppression have been widely reported for nanoparticle-reinforced organic coatings, where reduced permeability and improved microstructural stability delay rust propagation under salt-spray exposure.[24,37]

The ln L versus ln t plots in Figure 11 further elucidate rust-growth kinetics via the power-law relationship $L = kt^n$. The fitted exponents (n) and rate constants (k) summarized in Table 5 reveal distinct mechanistic regimes for each coating. The no-additive coating yields n ≈ 0.542, closely approximating the theoretical value of 0.5 expected for diffusion-controlled corrosion. This confirms that rust propagation is governed primarily by chloride-ion transport through a porous and weakly protective film.

The plant-extract coating exhibits a similar exponent (n ≈ 0.512) but with a reduced rate constant (k ≈ 0.291), indicating that phytochemicals slow corrosion kinetics without fundamentally altering the diffusion-controlled nature of the process. Such behaviour is consistent with adsorption-driven inhibition mechanisms, where polyphenols, alkaloids, and flavonoids form interfacial films that partially block active corrosion sites and suppress anodic/cathodic reactions.[8,14,17]

In contrast, the nanocomposite coating yields an exponent n ≈ 1.052 and an exceptionally small rate constant (k ≈ 0.004). The near-unity exponent suggests a shift from simple diffusion control toward a more barrier-limited or interface-controlled regime, where corrosion growth is constrained primarily by the integrity and adhesion of the nanocomposite film rather than ionic transport alone. This mechanistic transition reflects the synergistic role of Cu_2O nanoparticles in reinforcing coating cohesion, sealing micro-defects, and promoting passive-film formation at the metal/coating interface. Similar deviations from parabolic kinetics have been observed in advanced nanocomposite coatings exhibiting enhanced scribe-edge stability and delayed underfilm corrosion.[22,23,34]

Collectively, the kinetic analyses establish a clear mechanistic hierarchy: Nanocomposite coating > Plant-extract coating > No-additive coating. The plant extract improves corrosion resistance primarily through adsorption-driven film formation and surface passivation, thereby reducing corrosion rates while

preserving diffusion-controlled kinetics. However, the Cu_2O nanocomposite coating introduces an additional physical barrier mechanism, wherein nanoparticles increase diffusion tortuosity, densify the polymer network, and suppress underfilm delamination. The combined effects of chemical inhibition (from phytochemicals) and microstructural reinforcement (from Cu_2O) produce a highly compact and adherent coating capable of shifting corrosion kinetics toward a barrier-limited regime. These findings are in strong agreement with recent literature on green nanocomposite coatings, which consistently report suppressed rust-growth kinetics, reduced parabolic rate constants, and altered growth exponents relative to conventional organic inhibitors alone.[23,37] The exceptionally low k_p and k values observed for the nanocomposite system in this study underscore its effectiveness as a high-performance, eco-friendly corrosion-protection strategy for tin substrates in chloride-rich environments.

4. Conclusion

This study demonstrates the effectiveness of a green Cu_2O–*G. senegalensis* nanocomposite coating for enhancing corrosion protection of tin substrates in chloride environments. Phytochemical screening confirmed the presence of bioactive compounds such as tannins, flavonoids, glycosides, saponins, and carbohydrates in the aqueous extract, which contribute to adsorption-driven inhibition through formation of protective surface films. Gravimetric immersion tests revealed that incorporation of plant extract significantly reduced corrosion rates compared with the additive-free coating, while the Cu_2O nanocomposite system provided the most pronounced protection, achieving a minimum corrosion rate of approximately 0.17 mm y^{-1} at 1.0 wt% loading. Accelerated salt-spray exposure further confirmed the superior durability of the nanocomposite coating, which exhibited minimal rust propagation, rust-creep lengths below 2 mm, and corroded areas below 5%. Adsorption isotherm analysis indicated spontaneous inhibitor adsorption with predominantly physisorption interactions, while kinetic modelling showed a substantial reduction in corrosion propagation rates and a transition toward barrier-controlled protection. Overall, the synergistic combination of plant-derived phytochemicals and Cu_2O nanoparticles produces a compact, environmentally friendly coating capable of significantly improving corrosion resistance of tin in chloride-rich environments.

Conflict of Interest

The authors declare no conflict of interest.

References

1. M. Sheydaei, The use of plant extracts as green corrosion inhibitors: a review, *Surfaces*, **2024**, *7*, 380–403. https://doi.org/10.3390/surfaces7020024
2. U. S. Nwigwe and C. I. Nwoye, Green corrosion inhibitors for steel and other metals in basic media: a mini-review, *Res. Eng. Struct. Mater.*, **2023**. https://doi.org/10.17515/resm2023.643ma0116
3. J. O. Okeniyi, C. A. Loto and A. P. I. Popoola, *Morinda lucida* effects on steel-reinforced concrete in 3.5% NaCl: implications for corrosion protection of wind-energy structures, *Energy Procedia*, **2014**, *50*, 421–428. https://doi.org/10.1016/j.egypro.2014.06.051
4. K. A. Abdelshafeek, W. E. Abdallah, W. M. Elsayed, H. A. Eladawy and A. M. El-Shamy, *Vicia faba* peel extracts bearing fatty acids moieties as a cost-effective and green corrosion inhibitor for mild steel in marine water, *Sci. Rep.*, **2022**, *12*, 20611. https://doi.org/10.1038/s41598-022-24793-3
5. U. Samad, M. Alam, H. Abdo, A. Anis and S. Al-Zahrani, Synergistic effect of nanoparticles: enhanced mechanical and corrosion protection properties of epoxy coatings incorporated with SiO_2 and ZrO_2, *Polymers*, **2023**, *15*, 3100. https://doi.org/10.3390/polym15143100
6. B. E. A. Rani and B. B. J. Basu, Green inhibitors for corrosion protection of metals and alloys: an overview, *Int. J. Corros.*, **2012**, *2012*, 380217. https://doi.org/10.1155/2012/380217
7. B. R. Holla, R. Mahesh, H. R. Manjunath and V. R. Anjanapura, Plant extracts as green corrosion inhibitors for different kinds of steel: a review, *Heliyon*, **2024**, *10*, e33748. https://doi.org/10.1016/j.heliyon.2024.e33748
8. H. Parangusan, M. H. Sliem, A. M. Abdullah, M. Elhaddad, N. Al-Thani and J. Bhadra, Plant extract as green corrosion inhibitors for carbon steel substrate in different environments: a systematic review, *Int. J. Electrochem. Sci.*, **2025**, *20*, 100919. https://doi.org/10.1016/j.ijoes.2024.100919
9. I. Hassan, N. M. Baba, M. E. Benin and A. H. Labulo, Review on green synthesis of silica nanoparticle functionalized graphene oxide acrylic resin for anti-corrosion applications, *J. Umm Al-Qura Univ. Appl. Sci.*, **2024**, *10*, 379–39. https://doi.org/10.1007/s43994-023-00106-w
10. T.-R. Ovari, T. Toth, G. Katona, G. S. Szabó and L. M. Muresan, Epoxy coatings doped with (3-aminopropyl)triethoxysilane-modified silica nanoparticles for anti-corrosion protection of zinc, *Coatings*, **2023**, *13*, 1844. https://doi.org/10.3390/coatings13111844

11. J. E. D. López-Campos, J. Mojica-Gómez, A. Maciel-Cerda, V. M. Castaño and G. Hernández-Padrón, Hybrid epoxy–SiO_2/GO nanosheets anti-corrosive coating for aeronautic aluminum Al6061-T5, *J. Coat. Technol. Res.*, **2024**, *21*, 559–574. https://doi.org/10.1007/s11998-023-00838-8
12. M. Saikia, T. Dutta, N. Jadhav and D. J. Kalita, Insights into the development of corrosion protection coatings, *Polymers*, **2025**, *17*, 1548. https://doi.org/10.3390/polym17111548
13. F. Olivieri, F. Scherillo, R. Castaldo, M. Cocca, A. Squillace, G. Gentile and M. Lavorgna, Effectiveness of mesoporous silica nanoparticles functionalized with benzoyl chloride in pH-responsive anticorrosion polymer coatings, *ACS Appl. Polym. Mater.*, **2023**, *5*, 5917–5925. https://doi.org/10.1021/acsapm.3c00585
14. C. Verma, E. E. Ebenso, I. Bahadur and M. A. Quraishi, An overview on plant extracts as environmental sustainable and green corrosion inhibitors for metals and alloys in aggressive corrosive media, *J. Mol. Liq.*, **2018**, *266*, 577–590. https://doi.org/10.1016/j.molliq.2018.06.110
15. T. Izuagie, Y. Salihu, S. Umar and O. Oyekunle Akintola, Sustainable Nanohybrid Coating from Sugarcane-Bagasse Silica and F. sycomorus Extract for Long-Term Corrosion Resistance of Metal Surfaces, in *Proceedings of the 10th ACS Nigeria International Chemical Sciences Symposium*, ACS Nigeria, **2025**, pp. 159–168. https://doi.org/10.55455/acsnigeria.1.2.159-168
16. T. Izuagie, S. Umar and K. M. Bashar, Inhibition potential of extract of leaves of Sodom apple in the corrosion of mild steel in 1.0 M H_2SO_4, *Caliphate J. Sci. Technol.*, **2024**, *5*, 294–299. https://doi.org/10.4314/cajost.v5i3.7
17. A. Miralrio and A. Espinoza Vázquez, Plant extracts as green corrosion inhibitors for different metal surfaces and corrosive media: a review, *Processes*, **2020**, *8*, 942. https://doi.org/10.3390/pr8080942
18. O. O. Ogunleye, A. O. Arinkoola, O. A. Eletta, O. O. Agbede, Y. A. Osho, A. F. Morakinyo and J. O. Hamed, Green corrosion inhibition and adsorption characteristics of Luffa cylindrica leaf extract on mild steel in hydrochloric acid environment, *Heliyon*, **2020**, *6*, e03205. https://doi.org/10.1016/j.heliyon.2020.e03205
19. S. Bilgiç, Plant extracts as corrosion inhibitors for aluminium in acidic environments: review I, *Commun. Fac. Sci. Univ. Ank. Ser. B*, **2022**, *64* (1), 20–79.
20. C. A. Barbu, I. Fierascu, A. Semenescu and C. M. Cotrut, Critical review regarding the application of plant extracts as eco-friendly corrosion inhibitors: a sustainable interdisciplinary approach, *Molecules*, **2025**. https://doi.org/10.3390/molecules30183722
21. A. Dehghani, M. Zabihi-Gargari and M. T. Majd, Development of a nanocomposite coating with anti-corrosion ability using graphene oxide nanoparticles modified by Echium ammonium extract, *Prog. Org. Coat.*, **2022**, *166*, 106778. https://doi.org/10.1016/j.porgcoat.2022.106778
22. L. M. Muresan, Nanocomposite coatings for anti-corrosion properties of metallic substrates, *Materials*, **2023**, *16*, 5092. https://doi.org/10.3390/ma16145092
23. D.-I. Răuță, E. Matei and S.-M. Avramescu, Recent development of corrosion inhibitors: types, mechanisms, electrochemical behavior, efficiency, and environmental impact, *Technologies*, **2025**, *13*, 103. https://doi.org/10.3390/technologies13030103
24. M. Honarvar Nazari, Y. Zhang, A. Mahmoodi, G. Xu, J. Yu, J. Wu and X. Shi, Nanocomposite organic coatings for corrosion protection of metals: a review of recent advances, *Prog. Org. Coat.*, **2022**, *162*, 106573. https://doi.org/10.1016/j.porgcoat.2021.106573
25. M. G. Fontana, *Corrosion engineering*, 3rd edn, Tata McGraw-Hill, New Delhi, **2005**.
26. F. Onwuliri, J. Ndako, A. Olabode, G. Echeonwu, E. Onwuliri, P. Nwankiti, G. Salisu, M. Ohaeri and G. Amona, Phytochemical screening and antibacterial activity of Guiera senegalensis leaf extracts, *Int. J. Trop. Agric. Food Syst.*, **2009**. https://doi.org/10.4314/ijotafs.v3i2.50034
27. T. Izuagie, E. O. Meseke, S. S. Awala, M. A. Yahaya and A. Umar, Green nanopesticides from copper(I) oxide and neem seed oil: activity against cowpea weevil and mosquito larvae, *J. Chem. Soc. Niger.*, **2025**, *50*, 1064–1081. https://doi.org/10.4314/jcsn.v50i5.12
28. B. Mod, A. V. Baskar, R. Bahadur, E. Tavakkoli, L. Van Zwieten, G. Singh and A. Vinu, From cane to nano: advanced nanomaterials derived from sugarcane products with insights into their synthesis and applications, *Sci. Technol. Adv. Mater.*, **2024**. https://doi.org/10.1080/14686996.2024.2393568

29. ASTM International, Standard practice for operating salt spray (fog) apparatus, *ASTM B117-19*, ASTM International, West Conshohocken, PA, **2019**. https://doi.org/10.1520/B0117-19
30. ASTM International, Standard test method for evaluation of painted or coated specimens subjected to corrosive environments, *ASTM D1654-24*, ASTM International, **2024**. https://doi.org/10.1520/D1654-24
31. F. Bentiss, M. Traisnel and M. Lagrenée, The substituted 1,3,4-oxadiazoles: a new class of corrosion inhibitors of mild steel in acidic media, *Corros. Sci.*, **2000**, *42*, 127–146. https://doi.org/10.1016/S0010-938X(99)00049-9
32. A. Atkinson, Transport processes during the growth of oxide films at elevated temperature, *Rev. Mod. Phys.*, **1985**, *57*, 437–470. https://doi.org/10.1103/RevModPhys.57.437
33. N. Chakraborty, J. Banerjee, P. Chakraborty, A. Banerjee, S. Chanda, K. Ray, K. Acharya and J. Sarkar, Green synthesis of copper/copper oxide nanoparticles and their applications: a review, *Green Chem. Lett. Rev.*, **2022**, *15*, 187–215. https://doi.org/10.1080/17518253.2022.2025916
34. M. A. Deyab, M. M. Alghamdi, A. A. El-Zahhar and O. A. A. El-Shamy, Advantages of CoS_2 nanoparticles on the corrosion resistance and adhesiveness of epoxy coatings, *Sci. Rep.*, **2024**, *14*, 14684. https://doi.org/10.1038/s41598-024-64429-2
35. A. O. Okewale and A. T. Adebayo, Adsorption and thermodynamics studies of corrosion inhibition on carbon steel using pumpkin pod extract *(Telfairia occidentalis)*, *Arid Zone J. Eng. Technol. Environ.*, **2020**, *16*, 395–406.
36. A. A. Adamu, O. R. A. Iyun and J. D. Habila, Adsorption and thermodynamic studies of the corrosion inhibition effect of *Desmodium adscendens* extract on carbon steel in 2 M HCl, *BMC Chem.*, **2025**, *19*, 163. https://doi.org/10.1186/s13065-025-01541-y
37. R. Randis, D. B. Darmadi, F. Gapsari, A. A. Sonief, E. D. Akpan and E. E. Ebenso, The potential of nanocomposite-based coatings for corrosion protection of metals: a review, *J. Mol. Liq.*, **2023**, *390*, 123067. https://doi.org/10.1016/j.molliq.2023.123067

